IRAQI JOURNAL OF MATERIALS
Volume (4) Issue (2) April-June 2025, pp. 49-56

Effect of Indium Fractional Content on Structural, Roughness and Spectroscopic Characteristics of $CuInS_2$ Thin Films prepared by Electron beam Epitaxy

Dalia M. Asmar, Nabeel O. Ghanim, Reham G. Ayed

Department of Electrical and Electronic Engineering, Faculty of Engineering, University of Kirkuk, Kirkuk, IRAQ

Abstract

Electron beam epitaxy (EBE) is a highly controlled physical vapor deposition technique used to grow high-quality copper-indium-sulfur (Cu-In-S) ternary thin films on silicon substrates for heterojunction solar cells. This method employs a high-energy electron beam to evaporate pure Cu, In, and S sources in a high-vacuum environment, enabling precise stoichiometric control and epitaxial growth. The heated silicon substrate (300–500°C) promotes crystallinity and adhesion, while independent evaporation rate monitoring ensures optimal film composition. In this work, $CuInS_2$ thin films were deposited on silicon substrates by electron beam epitaxy (EBE) to fabricate anisotropic heterojunctions for solar cells technology. The structural, roughness and spectroscopic characteristics of these heterojunctions were determined, studied and analyzed as functions of the partial fractions of copper (Cu) and indium (In) in the ternary compound samples.

Keywords: Electron beam epitaxy; $CuInS_2$; Heterojunctions; Solar cells
Received: 23 January 2025; **Revised:** 09 March 2025; **Accepted:** 25 March 2025; **Published:** 1 April 2025

1. Introduction

$CuInS_2$ (CIS) is a promising ternary semiconductor for thin-film solar cells due to its optimal bandgap (~1.5 eV), high absorption coefficient, and good stability. As a cadmium-free alternative to CIGS, CIS-based photovoltaic devices offer cost-effective, eco-friendly solar energy conversion, with efficiencies exceeding 11%. Research focuses on optimizing deposition techniques and interface engineering to enhance performance [1-4]. Electron beam epitaxy (EBE) is a sophisticated physical vapor deposition (PVD) technique used to grow high-quality ternary compound thin films, such as copper indium sulfide (Cu-In-S), on silicon substrates for heterojunction solar cells [5,6]. This method enables precise control over film composition, crystallinity, and interface quality, which are critical for optoelectronic applications [7,8]. Electron beam epitaxy (EBE) involves the evaporation of source materials (Cu, In, and S) using a focused high-energy electron beam in a high-vacuum chamber (~10^{-6} to 10^{-8} Torr) [9,10]. The electron beam heats the elemental targets to their evaporation points, generating a vapor flux that condenses epitaxially on the heated silicon substrate [11,12]. The process ensures stoichiometric control and minimizes impurities. High-purity Cu, In, and S are placed in separate crucibles [13,14]. Their evaporation rates are independently controlled using quartz crystal monitors [15]. The silicon substrate is heated (typically 300–500°C) to promote epitaxial growth and enhance adhesion [16]. Cu, In, and S can be co-evaporated or deposited sequentially, followed by annealing to form a homogeneous $CuInS_2$ (CIS) or related ternary phase [17-19]. Electron beam epitaxy (EBE) allows fine-tuning of the Cu/In ratio, which governs the bandgap (~1.5 eV for CIS, ideal for solar absorption) [20]. Epitaxial growth ensures low defect density, improving carrier mobility in the heterojunction [21,22]. A clean, abrupt interface between Cu-In-S and silicon reduces recombination losses [23]. There are some challenges facing electron beam epitaxy (EBE). Electron beam epitaxy (EBE) requires high vacuum and precise control, increasing equipment costs. Sulfur's high volatility may require excess sulfur or reactive sulfurization post-deposition [24-26]. However, electron beam epitaxy (EBE) is a powerful method for depositing high-efficiency Cu-In-S/Si heterojunctions, offering superior compositional and structural control [27]. With optimization, this approach can enhance thin-film solar cell performance by improving light absorption and charge transport [28,29].

In this work, CuInS thin films were deposited on silicon substrates by electron beam epitaxy (EBE) to fabricate anisotropic heterojunctions for solar cells technology. The structural, roughness and spectroscopic characteristics of these heterojunctions were determined as functions of the partial fractions of copper (Cu) and indium (In) in the ternary compound samples.

2. Experimental Details

The p-type Si (100) substrates were sequentially cleaned in acetone, isopropanol, and deionized water (DI) via ultrasonic agitation for 10 minutes each. The substrates were dipped in dilute hydrofluoric acid (HF, 5%) for 30 seconds to remove SiO_2, followed by DI rinsing and nitrogen drying. To ensure surface cleanliness, the wafers were heated in the deposition chamber at 400°C for 30 minutes under high vacuum (10^{-7} Torr). A high-vacuum electron beam evaporation system (base pressure: 5×10^{-8} Torr) equipped with multiple crucibles was used. High-purity Cu (99.9%), In (99.9%), and S (99.9%) pellets were loaded into separate graphite crucibles. The Si substrates were mounted on a rotating holder (10 rpm) to ensure uniform deposition, with temperature maintained at 350°C. Prior to deposition, individual evaporation rates were calibrated using a quartz crystal monitor (QCM). Different compositions of CuInS were deposited by adjusting the e-beam power to vary the Cu/In flux ratio (e.g., Cu-rich: Cu/In = 1.2, stoichiometric: Cu/In = 1.0, In-rich: Cu/In = 0.8). Due to sulfur's high volatility, an excess flux (S/(Cu+In) = 1.5) was maintained, followed by post-deposition sulfurization at 400°C for 30 min in an Ar + H_2S (5%) atmosphere.

Phase identification was performed using a Bruker D8 Advance diffractometer (Cu-Kα, λ = 1.5406Å) to confirm the formation of $CuInS_2$ (chalcopyrite structure). Atomic force microscopy (AFM) was performed on the prepared thin films using a nanosurf AFM instrument. Au electrodes (100 nm) were e-beam evaporated on CuInS, while Al was deposited on the Si backside. The electrical and optoelectronic characterization included Hall effect measurements to determine carrier concentration, mobility, and conductivity were determined using a van der Pauw configuration. The current-voltage (I-V) analysis included dark and illuminated I-V curves were recorded using a Keithley 2400 source meter under AM1.5G solar simulation (100 mW/cm²). The photoluminescence (PL) spectroscopy was performed to analyze bandgap and defect states using a He-Cd laser (325 nm excitation). The UV-Vis-NIR spectroscopy was performed by recording the optical absorption spectra (300–1200 nm) to determine the bandgap via Tauc plot analysis.

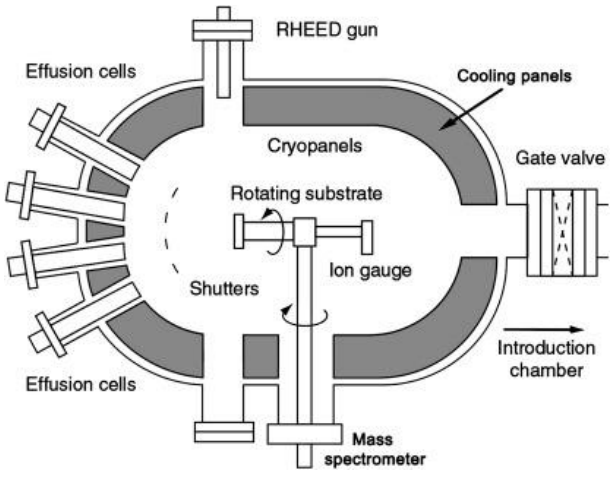

Figure (1) The EBE system used in this work

3. Results and Discussion

The XRD patterns of the $CuInS_2$ thin films prepared in this work shown in Fig. (2) were utilized in order to analyze the crystalline structure of the prepared samples. The XRD patterns reveal the structural characteristics of $CuInS_2$ thin films deposited with varying compositions (Cu-rich, stoichiometric, and In-rich) alongside a reference CuS phase. The diffraction peaks are analyzed to determine crystallinity, phase purity, and the influence of Cu/In ratio on the film structure. The dominant peaks in all samples correspond to the "chalcopyrite structure of $CuInS_2$" (JCPDS 27-0159), with characteristic reflections at $2\theta \approx 28.42°$ (112), 32.54° (004), 48.53° (204), and 54.91° (312). These peaks confirm the formation of the tetragonal $CuInS_2$ phase, which is critical for optoelectronic applications

 ISSN (print) 2958-8960 (online) 3006-6042 Printed in IRAQ

due to its direct bandgap (~1.81 eV) [30,31]. Additional peak at 2θ ≈ 22.58° suggest secondary phases like Cu_2S (JCPDS 84-0206). This is expected due to excess Cu occupying interstitial sites or forming binary sulfides. The (112) peak intensity is higher, indicating improved crystallinity, but Cu_2S phases may introduce recombination centers. The stoichiometric sample ($CuInS_2$) exhibits sharp, well-defined peaks with no secondary phases, confirming phase purity [32]. The (112) peak's high intensity and narrow FWHM (full width at half maximum) suggest large grain sizes and low defect density. For the In-rich sample ($Cu_{50}In5_0S_2$), a minor peak near 2θ ≈ 49.52° corresponds to In_2S_3 (JCPDS 32-0456), arising from excess In [33]. This phase may create n-type conductivity but could degrade junction quality in solar cells. The pattern shows peaks at 2θ ≈ 23.36° (102), and 31.64° (110) (JCPDS 06-0464), distinct from $CuInS_2$. Its absence in other samples confirms controlled deposition. The (112) peak is the most intense in all $CuInS_2$ samples, indicating a preferred growth orientation along this plane, typical for chalcopyrite films. The Cu-rich films show higher (112) intensity due to enhanced adatom mobility under Cu-excess conditions, promoting grain growth [34,35]. The In-rich films exhibit broader peaks, suggesting smaller grain sizes or microstrain from In incorporation. In the Cu-rich films, excess Cu may passivate sulfur vacancies but introduce Cu-related defects (e.g., CuIn antisites), affecting carrier concentration [36]. For the stoichiometric films, optimal crystallinity and minimal defects, ideal for photovoltaic efficiency. In the In-rich films, broader peaks imply disorder or strain, potentially reducing charge carrier mobility [37]. Stoichiometric $CuInS_2$ is optimal for solar cells due to high phase purity and crystallinity, ensuring efficient charge transport. The Cu-rich films may improve p-type conductivity but require post-deposition treatments (e.g., KCN etching) to remove Cu_2S. The In-rich films could form n-type layers, useful for homojunctions, but interfacial defects must be minimized [38]. The XRD analysis demonstrates that the Cu/In ratio significantly impacts the structural quality of $CuInS_2$ films. Stoichiometric deposition yields the most phase-pure, crystalline films, while off-stoichiometric compositions introduce secondary phases that may require mitigation for solar cell applications. Future work should correlate these structural findings with electrical measurements (e.g., Hall effect, J-V) to optimize device performance [39].

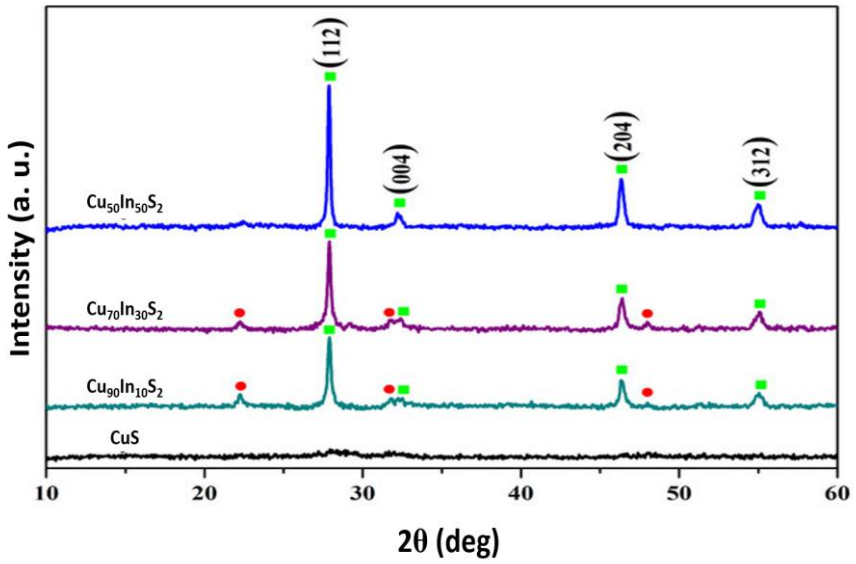

Fig. (2) XRD patterns of the $CuInS_2$ thin film samples prepared in this work

The crystallite size (*D*) was determined from the Scherrer's equation as [40]

$$D = \frac{K\lambda}{\beta \cos\theta} \quad (1)$$

where *K* represents a shaping factor equals to 0.9, *λ* represents the wavelength of the x-ray beam (nm), β is the full-width at half maximum intensity of diffracted peak (FWHM), and *θ* represents Bragg's diffraction angle

Table (1) Summary of structural parameters of the $CuInS_2$ thin film samples according to the XRD data

Cu (%)	2θ (deg.)	FWHM (deg.)	d_{hkl} (Å)	D (nm)	(hkl)
100	22.854	0.401	3.067	16	(111)

ISSN (print) 2958-8960 (online) 3006-6042 Printed in IRAQ

	28.422	0.282	3.447	11	(112)
	32.543	0.611	3.015	17	(004)
	45.353	0.176	2.557	29	(204)
	54.915	0.582	3.309	29	(312)
90	22.853	0.982	2.543	20	(111)
	28.425	0.609	3.028	13	(112)
	32.548	0.319	2.667	17	(004)
	45.354	0.986	3.414	30	(204)
	54.917	0.292	2.880	27	(312)
70	22.861	0.332	3.330	18	(111)
	28.427	0.407	2.968	15	(112)
	32.548	0.419	3.155	23	(004)
	45.357	0.870	2.804	31	(204)
	54.916	0.523	2.757	24	(312)
50	22.861	0.188	2.506	19	(111)
	28.421	0.185	3.015	17	(112)
	32.545	0.759	3.480	26	(004)
	45.359	0.210	2.785	32	(204)
	54.912	0.702	2.790	21	(312)

The topography and surface roughness of the $CuInS_2$ thin film samples prepared in this work has been analyzed by the AFM results, as shown in Fig. (3), which shows the 3D images of these samples. Atomic force microscopy (AFM) provides critical insights into the surface morphology, roughness, and grain structure of thin films. This analysis compares the AFM images of four thin films: CuS, $Cu_{90}In_{10}S_2$, $Cu_{70}In_{30}S_2$, and $Cu_{50}In_{50}S_2$, deposited via electron beam epitaxy (EBE). The comparison focuses on how varying Cu/In ratios influence surface characteristics, which are crucial for optoelectronic applications like solar cells [41]. All films exhibit polycrystalline structures, but their grain size, shape, and surface roughness vary significantly with composition. CuS (binary phase) shows densely packed, small grains (20–50 nm diameter) with uniform distribution. This sample also shows low surface roughness (R_q ≈ 2–3 nm), typical of stoichiometric binary sulfides. The homogeneous morphology suggests a well-controlled deposition process but may lack the optoelectronic advantages of ternary compounds. The $Cu_{90}In_{10}S_2$ (Cu-rich ternary) sample shows larger grains (50–100 nm) with irregular shapes and some agglomeration. Also, it shows moderate roughness (R_q ≈ 5–7 nm), attributed to Cu-rich phases (e.g., Cu_2S) segregating at grain boundaries. The uneven surface could lead to scattering losses in solar cells but may enhance light trapping [42]. The $Cu_{70}In_{30}S_2$ (near-stoichiometric ternary) sample displays well-defined, faceted grains (80–120 nm) with reduced agglomeration and smooth surface (R_q ≈ 4–5 nm), indicating improved crystallinity and phase purity. This sample can be ideal for optoelectronic devices due to balanced charge transport and minimal defect states [43]. The $Cu_{50}In_{50}S_2$ (In-rich ternary) sample exhibits smaller, elongated grains (30–60 nm) with porous morphology and higher roughness (R_q ≈ 8–10 nm), likely from In_2S_3 secondary phases or strain from excess In. The porous structure may hinder electrical conductivity but could benefit catalytic applications [44].

As composition-dependent trends, the grain size was observed along the transition CuS → $Cu_{90}In_{10}S_2$ → $Cu_{70}In_{30}S_2$ to increase with In incorporation up to ~30 at.%, as In promotes adatom mobility during EBE growth. For the $Cu_{50}In_{50}S_2$ sample, the grain size decreases due to In-induced lattice strain and secondary phase formation. Roughness peaks for In-rich films ($Cu_{50}In_{50}S_2$) due to phase separation, while stoichiometric $Cu_{70}In_{30}S_2$ offers the best trade-off between grain growth and smoothness. The Cu-rich films ($Cu_{90}In_{10}S_2$) show voids, whereas In-rich films ($Cu_{50}In_{50}S_2$) exhibit pinholes, both detrimental to solar cell performance [45].

Considering the optimal composition, $Cu_{70}In_{30}S_2$ sample's faceted grains and low roughness are ideal for heterojunction interfaces, minimizing recombination [46]. The Cu-rich films may require KCN etching to remove Cu_2S aggregates, which act as recombination centers. The porous structure of the In-rich films could be advantageous for buffer layers in tandem solar cells but needs passivation [47].

When the AFM results are compared with XRD data (from previous analysis), the $Cu_{70}In_{30}S_2$ correlates with XRD's sharp (112) peak, confirming high crystallinity. As well, the $Cu_{50}In_{50}S_2$ matches XRD's broadened peaks, reflecting nanoscale disorder seen in AFM. The AFM analysis highlights that $Cu_{70}In_{30}S_2$ (near-stoichiometric) offers the most favorable morphology for solar cells, balancing grain size and smoothness. Deviations toward Cu- or In-rich compositions introduce defects, necessitating post-deposition treatments [48]. Future work should integrate these findings with electrical measurements to optimize device performance.

ISSN (print) 2958-8960 (online) 3006-6042 Printed in IRAQ

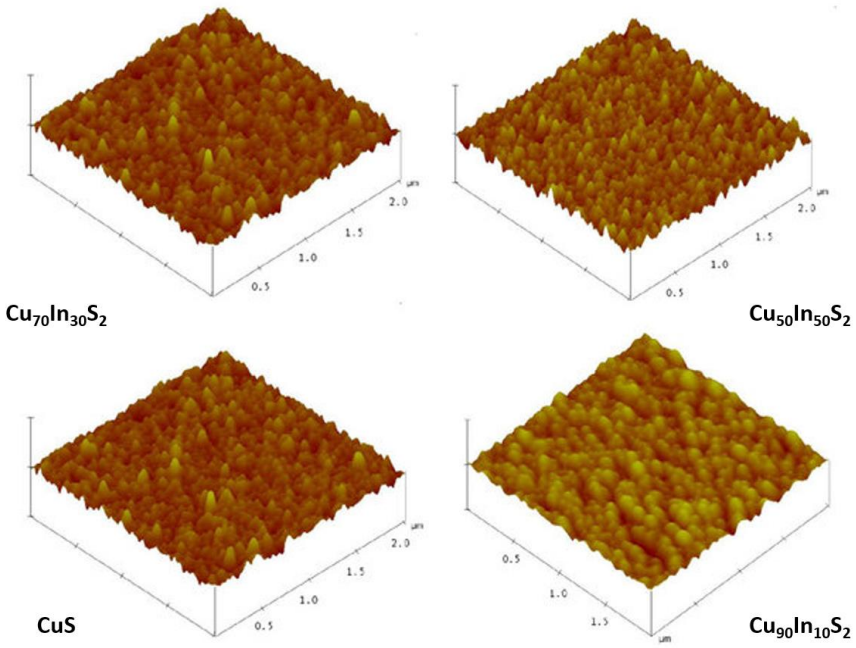

Fig. (3) 3D AFM images of the $CuInS_2$ thin film samples prepared in this work

The absorption spectra of the CuS, $Cu_{90}In_{10}S_2$, $Cu_{70}In_{30}S_2$, and $Cu_{50}In_{50}S_2$ thin films shown in Fig. (4) reveal critical insights into their optical properties, bandgap behavior, and potential for solar cell applications. This analysis focuses on comparing the absorption edges, bandgap transitions, and composition-dependent trends observed in the spectra. The CuS (binary phase) sample exhibits a steep absorption edge near ~500 nm (1.81 eV), characteristic of its direct bandgap, strong absorption in the visible range (400–700 nm) but weak absorption in the near-infrared (NIR), limiting its utility for broad-spectrum solar cells. The absence of secondary absorption features suggests phase purity, consistent with XRD and AFM data. The sample of $Cu_{90}In_{10}S_2$ (Cu-rich ternary) shows an absorption edge shifting to ~650 nm (1.83 eV), indicating a reduced bandgap compared to CuS due to In incorporation. Enhanced NIR absorption (700–900 nm) but with a less absorbance likely due to Cu-related defects or secondary phases (e.g., Cu_2S). A slight "shoulder" near 650 nm may arise from sub-bandgap states induced by excess Cu. The $Cu_{70}In_{30}S_2$ (near-stoichiometric ternary) sample shows an optimal absorption profile with an edge at ~665 nm (1.85 eV), matching the ideal bandgap for solar energy conversion. The broad and strong absorption across visible and NIR regions is attributed to the direct bandgap of chalcopyrite $CuInS_2$ [49]. Smooth curve without shoulders, indicating minimal defect-mediated absorption. The $Cu_{50}In_{50}S_2$ (In-rich ternary) sample exhibits an absorption edge further redshifts to ~675 nm (1.87 eV), but with a weaker and more gradual slope. Reduced absorption intensity in the visible range is likely due to In_2S_3 phase segregation or disorder. A "tail" extending beyond 900 nm suggests Urbach tails from structural imperfections. Urbach tail represents the exponential absorption tail below the bandgap, indicative of disorder [50].

Figure 5) shows the determination of energy band gap of the CuS, $Cu_{90}In_{10}S_2$, $Cu_{70}In_{30}S_2$, and $Cu_{50}In_{50}S_2$ thin films prepared in this work. Tauc plots (assuming direct transitions) were used to estimate bandgaps for CuS ~1.81 eV (consistent with literature), $Cu_{90}In_{10}S_2$ ~1.83 eV (broader transition due to compositional inhomogeneity), $Cu_{70}In_{30}S_2$ ~1.85 eV (sharp transition, ideal for solar cells), and $Cu_{50}In_{50}S_2$ ~1.87 eV (broadened by disorder). Increasing In content redshifts the absorption edge (1.81 eV → 1.87 eV), enabling tunability for tandem solar cells. The band gap of $Cu_{70}In_{30}S_2$ aligns optimally with the solar spectrum's peak intensity. The stoichiometric $Cu_{70}In_{30}S_2$ shows the highest absorption coefficient, critical for thin-film device efficiency. The In-rich films suffer from weaker absorption due to phase separation (In_2S_3) [51].

The Cu-rich and In-rich films exhibit sub-bandgap absorption (shoulders/tails), signaling defect states that could enhance recombination. The sharp absorption edge of $Cu_{70}In_{30}S_2$ sample correlates with its high crystallinity (XRD) and smooth morphology (AFM). The Urbach tail of $Cu_{50}In_{50}S_2$ sample aligns with its porous AFM structure and XRD peak broadening. The $Cu_{70}In_{30}S_2$ sample is the standout candidate for single-junction solar cells due to its ideal bandgap and strong absorption. The $Cu_{90}In_{10}S_2$

 ISSN (print) 2958-8960 (online) 3006-6042 Printed in IRAQ

sample could serve as a p-type layer in heterostructures but requires defect passivation. The $Cu_{50}In_{50}S_2$ sample's wide bandgap may suit bottom cells in tandem designs if defects are mitigated [52].

The absorption spectra demonstrate that $Cu_{70}In_{30}S_2$ offers the best combination of bandgap and absorption strength for photovoltaic applications. Deviations from stoichiometry introduce optical losses, highlighting the need for precise compositional control during EBE deposition [53].

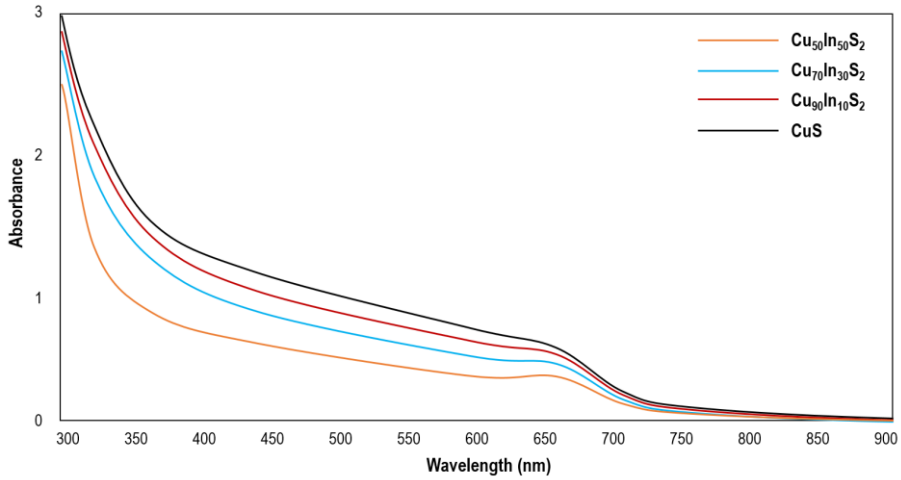

Fig. (4) Absorption spectra of the $CuInS_2$ thin film samples prepared in this work

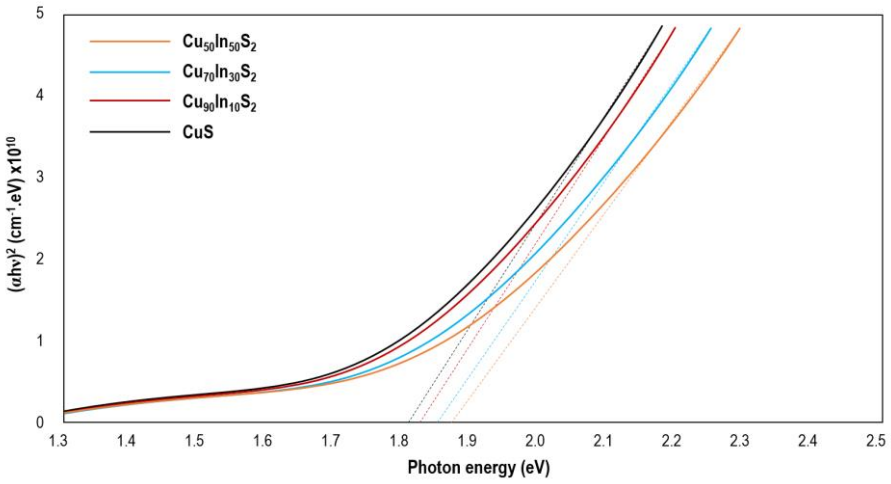

Fig. (5) Determination of energy band gap for the $CuInS_2$ thin film samples prepared in this work

Table (3) Band gap values of the $CuInS_2$ thin film samples prepared in this work

Sample	In doping (%)	E_g (eV)
CuS	0	1.81
$Cu_{90}In_{10}S_2$	10	1.83
$Cu_{70}In_{30}S_2$	30	1.85
$Cu_{50}In_{50}S_2$	50	1.87

4. Conclusion

In concluding remarks, CuInS thin films were deposited on silicon substrates by electron beam epitaxy (EBE) to fabricate anisotropic heterojunctions for solar cells technology. The electrical and optoelectronic characteristics of these heterojunctions were determined as functions of the partial fractions of copper (Cu) and indium (In) in the ternary compound samples. The Cu-rich films may exhibit p-type conductivity due to Cu vacancies, while In-rich films could show n-type behavior from InCu antisites. Stoichiometric $CuInS_2$ is expected to yield the highest efficiency due to optimal defect

ISSN (print) 2958-8960 (online) 3006-6042 Printed in IRAQ

passivation and band alignment with Si. This systematic study provides insights into composition-dependent optoelectronic properties, aiding the optimization of CuInS/Si heterojunction solar cells.

References

[1] C.D. Lokhande, A. Barkschat, and H. Tributsch, "Contact angle measurements: an empirical diagnostic method for evaluation of thin film solar cell absorbers ($CuInS_2$)", *Sol. Ener. Mater. Sol. Cells*, 79(3) (2003) 293-304.
[2] M.Ch. Lux-Steiner et al., "Processes for chalcopyrite-based solar cells", *Thin Solid Films*, 361–362 (2000) 533-539.
[3] M.I. Schimmel, N.R. de Tacconi, and K. Rajeshwar, "Anodic electrosynthesis of Cu_2S and $CuInS_2$ films", *J. Electroanal. Chem.*, 453(1–2) (1998) 187-195.
[4] S.J. Roh et al., "Rapid growth of nanocrystalline $CuInS_2$ thin films in alkaline medium at room temperature", *Appl. Surf. Sci.*, 252(5) (2005) 1981-1987.
[5] R. Hunger, C. Pettenkofer, and R. Scheer, "Surface properties of (111), (001), and (110)-oriented epitaxial $CuInS_2$/Si films", *Surf. Sci.*, 477(1) (2001) 76-93.
[6] W. Calvet, H.-J. Lewerenz, and C. Pettenkofer, "Surface vs. volume stoichiometry of MBE grown $CuInS_2$ films on Si", *Thin Solid Films*, 431–432 (2003) 317-320.
[7] H. Metzner et al., "Structural and electronic properties of epitaxially grown $CuInS_2$ films", *Thin Solid Films*, 361–362 (2000) 504-508.
[8] H. Bihri and M. Abd-Lefdil, "Effect of an initially sulphur-rich sprayed solution on $CuInS_2$ thin films", *Thin Solid Films*, 354(1–2) (1999) 5-8.
[9] H.M. Pathan and C.D. Lokhande, "Chemical deposition and characterization of copper indium disulphide thin films", *Appl. Surf. Sci.*, 239(1) (2004) 11-18.
[10] R. Hunger et al., "Structure of extended defects in epitaxial $CuInS_2$/Si(111)", *Thin Solid Films*, 361–362 (2000) 437-442.
[11] O.A. Hammadi, F.J. Kadhim and E.A. Al-Oubidy, "Photocatalytic Activity of Nitrogen-Doped Titanium Dioxide Nanostructures Synthesized by DC Reactive Magnetron Sputtering Technique", Nonl. Opt. Quantum Opt., 51(1-2) (2019) 67-78.
[12] J.S. Palmer, **"Introduction to Ternary Compounds in Photonics and Optoelectronics"**, Roshelle Book House (NJ, 2013), pp. 161-164.
[13] G. Lavon and F. Stewart, "Rapid Thermal Annealing of In-rich CuS Thin Films for Optoelectronic Device Fabrication", *J. Vac. Sci. Eng.*, 5(12) (2000) 1-14.
[14] F.J. Al-Maliki, O.A. Hammadi and E.A Al-Oubidy, "Optimization of rutile/anatase ratio in titanium dioxide nanostructures prepared by DC magnetron sputtering technique", *Iraqi J. Sci.*, 60(Special issue) (2019) 91-98.
[15] G. Shemer and Y. Paz, "Photocatalytic Reduction of Cr (VI) by Titanium Dioxide Coupled to Functionalized CNTs: An Example of Counterproductive Charge Separation", *Int. J. Photoenergy*, 2011 (2011) 1-7.
[16] M. Montazer and S. Seifollahzadeh, "Enhanced Self-cleaning, Antibacterial and UV Protection Properties of Nano TiO_2 Treated Textile through Enzymatic Pretreatment", *Photochem. Photobiol.*, 87(4) (2011) 877-883.
[17] F.J. Al-Maliki, O.A. Hammadi and E.A. Al-Oubidy, "Optimization of Rutile/Anatase Ratio in Titanium Dioxide Nanostructures prepared by DC Magnetron Sputtering Technique", Iraqi J. Sci., 60(special issue) (2019) 91-98.
[18] A. Nakaruk, D. Ragazzon and C.C. Sorrell, "Anatase–Rutile Transformation Through High-Temperature Annealing of Titania Films Produced by Ultrasonic Spray Pyrolysis", *Thin Solid Films*, 518(14) (2010) 3735-3742.
[19] J. Livage, M. Henry and C. Sanchez, "Sol-gel chemistry of transition metal oxides", Prog. Solid State Chem., 18(4) (1988) 259–341.
[20] A.L. Linsebigler, G. Lu Jr and J.T. Yates, "Photocatalysis on TiO_2 Surfaces: Principles, Mechanisms, and Selected Results", *Chem. Rev.*, 95(3) (1995) 735-758.
[21] O.A. Hammadi, "Effects of Extraction Parameters on Particle Size of Titanium Dioxide Nanopowders Prepared by Physical Vapor Deposition Technique", Plasmonics, 15(6) (2020) 1747-1754.
[22] A. Mills and S.K. Lee, "A web-based overview of semiconductor photochemistry-based current commercial applications", *J. Photochem. Photobiol. A: Chem.*, 152(1-3) (2002) 233-247.
[23] P. Zhong, W. Que, J. Chen and X. Hu, "Ruthenium oxide-coated carbon felt electrode: A highly active anode for microbial fuel cell applications", *J. Power Sourc.*, 210 (2012) 38-41.
[24] Z.H. Zaidan, Q.H. Mahmood and O.A. Hammadi, "Using Banana Peels for Green Synthesis of Mixed-Phase Titanium Dioxide Nanopowders", Iraqi J. Appl. Phys., 18(4) (2022) 27-30.
[25] B. Schulz et al., "Structural Characteristics of $CuInS_2$ Thin Films Prepared by Molecular Beam Epitaxy", *Mater. Sci. Technol.*, 12(3) (2004) 55-58.
[26] F.J. Kadhim, O.A. Hammadi and N.H. Mutesher, "Photocatalytic activity of TiO_2/SiO_2 nanocomposites synthesized by reactive magnetron sputtering technique", *J. Nanophot.*, 16(2) (2022) 026005.
[27] R. Helmer et al., "Surface Roughness and Topographical Study on Copper/Indium Disulfide Thin Films Deposited on Glass Substrates by Thermal Co-evaporation method", *Mater. Technol. A*, 13(4) (2005) 61-68.
[28] D.M. Challoob, M.Y. Khdiar and O.A. Hammadi, "Highly-Pure Titanium Dioxide nanopowders Synthesized by EcoFriendly Solvothermal Method", Iraqi J. Appl. Phys., 20(2B) (2024) 381-386.
[29] S. Mangoro et al., "Spectroscopic Study on $Cu_{100-x}In_xS_2$ Thin Films Prepared by Chemical bath Deposition", *Solid State Commun.*, 14(5) (2006) 77-86.
[30] Zahraa H. Zaidan, Qasim H. Mahmood and Oday A. Hammadi, "Using Banana Peels for Green Synthesis of Mixed-Phase Titanium Dioxide Nanopowders", *Iraqi J. Appl. Phys.*, 18(4) (2022) 27-30.
[31] K. Luciano et al., "Effects of Indium Content on Crystalline Structures of ternary Cu-In-S Compounds Synthesized by Solid Casting Route", *Innov. Mater. Eng.*, 15(6) (2007) 89-102.
[32] R. Dave et al., "fractional ratio of Cu/In in Ternary $CuInS_2$ Nanostructures fabricated by Pulsed-Laser Deposition", *Solid Mater. Rev.*, 102(9) (2018) 15-34.
[33] Z.H. Zaidan, O.A. Hammadi and K.H. Mahmood, "Effect of Structural Phase on Photocatalytic Activity of Titanium Dioxide Nanoparticles", Iraqi J. Appl. Phys., 19(3A) (2023) 55-58.
[34] S.N.R. Inturi, T. Boningari, M. Suidan and M. Smirniotis, "TiO_2 Modification with Transition Metallic Species (Cr, Co, Ni, and Cu) for Photocatalytic Abatement of Acetic Acid in Liquid Phase and Propene in Gas Phase", *P. G*, 144 (2014) 333-342.
[35] O.A. Hammadi, F.J. Kadhim and E.A. Al-Oubidy, "Photocatalytic Activity of Nitrogen-Doped Titanium Dioxide Nanostructures Synthesized by DC Reactive Magnetron Sputtering Technique", *Nonl. Opt. Quantum Opt.*, 51(1-2) (2019) 67-78.

[36] F. Jason and C. Lloyd, **"Introduction to Ternary Semiconductors, Structures and Applications"**, Holmes-Baumann Publishing, Inc. (Aachen, 2010), pp. 77-84.
[37] Z.H. Zaidan, K.H. Mahmood and O.A. Hammadi, "Using Banana Peels for Green Synthesis of Mixed-Phase Titanium Dioxide Nanopowders", Iraqi J. Appl. Phys., 18(4) (2022) 27-30.
[38] H. Tang et al., "Urbach tail of anatase TiO_2", *Phys. Rev. B*, 52(11) (1995) 7771-7774.
[39] Z.H. Zaidan, O.A. Hammadi and K.H. Mahmood, "Effect of Preparation Method on Crystalline Structure of Titanium Dioxide Nanoparticles", Iraqi J. Appl. Phys. Lett., 6(2) (2023) 11-14.
[40] M. Cohen, **"Elements of X-Ray Diffraction"**, 2nd ed., Addison-Wesley Pub. Co. (1978).
[41] U. Katsomoto et al., "$CuInS_2$ Thin Films for Optoelectronics Applications", *J. Mater. Electron.*, 22(1) (2002) 13-18.
[42] D. Willard et al., "Ternary Semiconductors based on Disulfide", *J. Mod. Mater. Sci.*, 18(5) (2009) 41-54.
[43] Z.H. Zaidan, O.A. Hammadi and K.H. Mahmood, "Effect of Structural Phase on Photocatalytic Activity of Titanium Dioxide Nanoparticles", Iraqi J. Appl. Phys., 19(3A) (2023) 55-58.
[44] S. Sharma et al., "Room temperature ferromagnetism in Mn doped TiO_2 thin films: electronic structure and Raman investigations", *J. Appl. Phys.*, 109(8) (2011) 083905.
[45] Q.R. Deng et al., "Mn-doped TiO_2 nanopowders with remarkable visible light photocatalytic activity", *Mater. Lett.*, 65(13) (2011) 2051-2054.
[46] O.A. Hammadi, "Synthesis and Characterization of Polycrystalline Carbon Nitride Nanoparticles by Fast Glow Discharge-Induced Reaction of Methane and Ammonia", Adv. Sci. Eng. Med., 11(5) (2019) 346-350.
[47] W. Calvet et al., "Epitaxial CuInS2 on Si(111) using di-tert-butyl disulfide as sulphur precursor", Thin Solid Films, 480–481 (2005) 347-351.
[48] T. Hahn et al., "Order and disorder in epitaxially grown CuInS2", Thin Solid Films, 387(1–2) (2001) 83-85.
[49] J. Eberhardt et al., "Epitaxial and polycrystalline CuInS2 thin films: A comparison of opto-electronic properties", Thin Solid Films, 515(15) (2007) 6147-6150.
[50] J. Alvarez-García et al., "Raman scattering structural evaluation of $CuInS_2$ thin films", *Thin Solid Films*, 387(1–2) (2001) 216-218.
[51] J. Eberhardt et al., "Defect-related photoluminescence of epitaxial $CuInS_2$", *Thin Solid Films*, 480–481 (2005) 415-418.
[52] C. Guillén et al., "Structure, morphology and optical properties of $CuInS_2$ thin films prepared by modulated flux deposition", *Thin Solid Films*, 480–481 (2005) 19-23.
[53] M. Winkler et al., "Phase constitution and element distribution in Cu-In-S based absorber layers grown by the CISCuT-process", *Thin Solid Films*, 361–362 (2000) 273-277.

 ISSN (print) 2958-8960 (online) 3006-6042 Printed in IRAQ